Egypt. J. Chem. Vol. 67, SI: M. R. Mahran, pp. 643 -653 (2024)

Egyptian Journal of Chemistry

http://ejchem.journals.ekb.eg/

Biochar from agricultural waste as promising sustainable filler for ethylene-propylene-diene composites

Samaa R. Salem[1], M.E. Abd El-Aziz[1,*], Adel A. Koriem[1], Gamal Turky[2], Ahmed I. Hussain[1]

[1] *Polymers and Pigments Department, National Research Centre, 33 El Bohouth St., Dokki, Giza, P.O. 12622, Egypt.*

[2] *Microwave Physics & Dielectrics Department, National Research Centre (NRC), 33 El Bohouth St., Dokki, Giza, P.O.12622, Egypt.*

Abstract

In this study, surface functionalized biochar (Bi) has been examined as a potential alternative to carbon black (HAF) and was used as filler for ethylene-propylene-diene monomer (EPDM) rubber. The influence of surface-treated biochar on the electrical conductivity, oxygen and water permeability, rheological characteristics, and mechanical properties of the elastomer was subsequently assessed in comparison to conventional fillers (HAF) commonly used in rubber applications. The study aims to delineate the key characteristics of the EPDM composites while the effect of the varying ratios of HAF and MBi to elastomers was assessed. Hence, the utilization of environmentally friendly filler extracted from agricultural waste of citrus trees presents a dual advantage: it diminishes the prevalence of citrus tree waste and serves as a sustainable substitute and filler in EPDM to curtail the reliance on common HAF. This strategic incorporation not only contributes to alleviating HAF usage but also elevates the overall quality of rubber-based products, aligning with a commitment to sustainable and eco-conscious manufacturing practices. Moreover, the dielectric spectroscopy and AC-conductivity investigations evidenced that all the obtained composites exhibited an insulator behaviour, which paves the way for a breakthrough in electrical technology.

Keywords: Biochar; carbon black; EPDM; dielectric properties; sustainable fillers

1. Introduction

Rubber materials play a pivotal role across diverse industrial domains, finding applications in water system gaskets, hoses, cable seals, profiles, roofing membranes, and seals for vehicles and aircraft doors and windows. Additionally, they serve as protective coverings for irrigation systems, owing to their cost-effectiveness, adaptability, and resilience in challenging conditions [1]. In the manufacturing of rubber composites, a myriad of inorganic fillers and organic components are employed. The characteristics of these filler particles wield significant influence over the stability of rubber composites. Some particles catalyse deterioration, while others act as barriers to oxygen flow, thereby retarding the degradation process of rubber composites [2, 3]. The nuanced nature of these filler materials underscores their crucial role in shaping the overall performance and longevity of rubber-based products.

As a key filler in rubber composite manufacturing, carbon black stands out and its predominant derivation from non-renewable sources such as tar, coal, acetylene, and natural gas raises environmental concerns. The production process of carbon black is notably detrimental to human health, releasing substantial amounts of carbon dioxide. This has spurred a recent trend towards seeking alternatives to carbon black—namely, eco-friendly and sustainable fillers. This shift reflects a broader commitment to reducing environmental impact and embracing materials that align with contemporary sustainability objectives [4, 5].

Ethylene-propylene-diene monomer (EPDM) rubber is renowned for its exceptional mechanical properties and wide operational temperature range [6]. Furthermore, the nonpolar EPDM stands out as a highly saturated elastomer with a minimal concentration of nonconjugated dienes, endowing it with excellent anti-aging characteristics, decent electrical resistivity, and resilience against weathering, oxidation, and chemical exposure [7]. Extensive research has explored the intricate relationships among the rheological, morphological, physical, and mechanical attributes of EPDM composites. It was revealed that the introduction of inorganic fillers into elastomers represents a strategic enhancement like

*Corresponding author e-mail: Mahmoud_essam12@yahoo.com.; (Mahmoud Essam Abd El-Aziz).
Receive Date: 27 February 2024, Revise Date: 26 April 2024, Accept Date: 15 May 2024
DOI: 10.21608/EJCHEM.2024.273133.9392

bolstering thermal and mechanical properties [8-10]. Notable examples of multifunctional inorganic fillers, doubling as compatibilizers, include carbon black (HAF), silica, $CaCO_3$, clay, zeolite, and organoclay [11-13]. Although carbon black remains the common reinforcing filler in the rubber industry, its inherent pernicious properties being carcinogenic and petroleum-based, have prompted exploration into alternative fillers. This quest has led to investigations into organo-montmorillonite, mica, bio-based fibers, and biochar as promising substitutes, addressing concerns related to cost, color limitations, and environmental impact associated with conventional fillers.

Biochar is a high-carbon source obtained from a waste-derived substance. Lately, a lot of researchers have been interested in the development of sustainable and low-carbon materials improved with biochar. Because of its porous structure and highly functionalized surface, biochar is compatible with several materials such as cement, asphalt, and polymer materials [14-16]. Biochar can be applied in many filed as crop production, water purification, air purification, catalyst, biogas production, fuel cell technology, electrochemical capacitor, and hydrogen storage [17-22].

As a pivotal tool in unraveling the intricate dynamics of polymeric systems stands a technique such as Broadband Dielectric Spectroscopy (BDS) [23]. This sophisticated instrument empowers researchers to delve into the realms of interfacial polarization within diverse systems characterized by heterogeneous structures. It provides invaluable insights into the mechanisms governing charge transport, thereby elucidating the conductivity phenomena. Moreover, BDS facilitates a nuanced exploration of relaxation dynamics at the molecular scale. In the context of rubber varieties, the conductivity and dielectric characteristics assume paramount significance. These properties not only serve as key benchmarks for understanding the material's behaviour but also serve as guiding metrics for directing research endeavors. The profound insights garnered through BDS in the realm of rubber varieties pave the way for prospective applications across a spectrum of industries, underscoring its role as a cornerstone in advancing materials science and engineering [24-26].

Herin, the modified biochar (MBi) was acquired through a sophisticated chemo-mechanical process employing stearic acid. The biochar itself originated from the pyrolysis of citrus trees. The dispersion of MBi within EPDM would act alternatively with carbon black. The mechanical properties of EPDM composites as well as the morphology and thermal analysis of obtained composites were investigated. This tailored treatment holds the promise of optimizing the synergism of MBi within the nonpolar elastomer composite, thereby potentially elevating its overall performance.

2. Material and Experimental Techniques

2.1 Materials

Ethylene-propylene-diene monomer (EPDM) acquired from Nasr Company, Egypt. Technical grade materials such as sulphur (S), zinc oxide (ZnO), stearic acid, phenyl-β-naphthyl amine (PBN), and N-cyclohexyl-2-benzothiazole sulphenamide (CBS) were acquired from a local rubber company. From Alexandria Carbon Black, Egypt, the carbon black (HAF) was provided where its specific gravity is 1.78 ± 0.1 and pH is 9 ± 0.5. All chemicals were used as it is without any purification.

2.2 Methods and Experiments

2.2.1. Preparation of biochar

Citrus tree stem pruning was first cleaned and then oven-dried for eight hours at 105 °C. After that, the pyrolysis was done under nitrogen gas in a muffle furnace at 450 °C where the temperature was superfatted at a rate of 10 °C per minute. It was then allowed to remain at this temperature for an hour before cooling. In a tumbling mill, the obtained Bi was pulverized and then sieved using a 170-mesh sieve.

2.2.2 Manufacture of modified biochar (MBi)

The stearic acid was used to change the biochar's chemical composition to boost its hydrophobicity. Firstly, the stearic acid (2 g) was dissolved in 100 ml of toluene, after that, a specific weight of Bi (100 g) was supplemented, and stirring was done for 24 hours. Ultimately, filtration and grinding were used to get the MBi, which was then dried at 75 °C in an oven till a constant weight was achieved. The MBi was kept in sealed plastic containers to keep it dry.

2.2.3 Mixing and Vulcanization

The materials for the rubber were thoroughly mixed in a laboratory two-roll mill with a diameter of 470 mm and a working distance of 300 mm. The slow roller has a gear ratio of 1:1.4, and its speed is 24 rev/min. The process of vulcanization was executed in a platen press that was heated to 162 ºC and operated at approximately 4 MPa of pressure. The rubber composite formulations and recommended cure periods are shown in **Table 1**.

2.3. Characterization:

A particle size analyzer (Nano-ZS, Malvern Instruments Ltd., UK) was applied to demonstrate the zeta potential and particle size distribution of the prepared fillers.

An OCA 15 EC (Germany) was used to determine the water contact angle for samples after 60 seconds of applying drops of 10 μL of triple distilled water.

A Shimadzu 8400S FTIR Spectrophotometer was used to record the 400–4000 cm^{-1} FTIR spectra of the as-prepared materials.

The Monsanto Oscillating Disc Rheometer model-100 was used to evaluate the following rheometric characteristics: minimum torque (ML), maximum

torque (MH), optimal cure time (tC90), scorch time (tS2), and the cure rate index (CRI) by ASTM standard D 2084-10.

The as-prepared samples' surface morphology was observed using a scanning electron microscope (SEM; JSM 6360LV, JEOL/Noran).

Water Vapor Permeability Analyzer (GBPI W303-B; China) was performed to measure the water vapor transmission rate (WVTR) at 38 °C, which used the cup method under specific humidity (4 %-10%) according to ISO 2528, ASTM D1653, and ASTM E96. Gas Permeability Analyzer (N530-B; China) was applied to evaluate the oxygen transmission rate (OTR) according to ASTM ISO2556-2001 and D1434-82 (2003).

The thermogravimetric analyzer (Shimadzu TGA-50, Columbia, EUA), at a heating rate of 10 °C/min in a nitrogen environment, was Utilized to perform the thermal analysis in the range of ambient temperature to 700 °C.

The sound absorption coefficient is obtained using two microphone impedance tube types B & K 4206 over a frequency range of 100–6400 Hz.

2.4. Physico-mechanical properties

2.4.1 The mechanical properties

Tensile and elongation were determined using a Zwick tensile testing machine (model-1425), according to ASTM D 412-10.

2.4.2 Swelling properties

The rubber composite swelling value (S.V.) was measured in toluene according to ASTM D 471-12a using the following equation:

$$S.V.\% = \left[\frac{w_i - w_0}{w_0}\right] \qquad \textbf{Eq. 1}$$

Wherein, Wo= weight before swelling and Wi = weight after swelling.

Moreover, Ahmed et al. [27] reported that the mass difference between the sample prior to (M1) and following (M2) extraction in toluene was used to calculate the soluble fraction (SF), as outlined in the following manner:

$$\%SF = \frac{M_1 - M_2}{M_1} \times 100 \qquad \textbf{Eq. 3}$$

2.4.3 Thermal oxidative aging

It was carried out according to ASTM D 573-10 at 90° C for different periods of up to 7 days in a good air circulation electric oven. The mechanical attributes of each specimen were systematically evaluated following a 24-hour aging test. Tensile strength, elongation at break, modulus, and the soluble fraction of the EPDM composites were analyzed post-aging to assess their resistance to aging. The retention percentage for the samples is computed using the following method [28]:

$$\%\,Retention = \frac{value\ after\ aging}{value\ before\ aging} \times 100 \qquad \textbf{Eq. 2}$$

2.5 Electrical and dielectric investigations

Dielectric properties of the investigated samples were achieved using a high-resolution Alpha-analyzer (NOVOCONTROL Technologies GmbH & Co. KG) at frequencies ranging from 10^{-1} to 10^{7} Hz. The two brass electrodes that make up the sample cell for these measurements are the upper electrode, which has a diameter of 20 mm, and the lower electrode, which is the spectrometer ground plate, has a diameter of 40 mm. The sample is sandwiched between them in the parallel plate geometry configuration. This is utilized to determine the complex dielectrics function $\varepsilon^*(\omega) = \varepsilon'(\omega) - \varepsilon''(\omega)$, where the real part, ε' is the permittivity and the imaginary part, ε'' is the dielectric loss. This complex dielectric function is equivalent to the complex conductivity function $\sigma*(\omega) = \sigma'(\omega) + \sigma''(\omega)$ where $\sigma^*(\omega) = i\omega\varepsilon_o\varepsilon^*(\omega)$, implying that $\sigma' = \varepsilon_o\omega\varepsilon''$ and $\sigma'' = \varepsilon_o\omega\varepsilon'$ ($\varepsilon_o$being the vacuum permittivity).

3 Results and Discussion

3.1 Characterizations of fillers

Fig. 1 displays the FTIR spectra of Bi for the MBi and HAF. It was shown that identification bands at 1620 and 1040 cm^{-1} were present for all filler types utilized which related to C=C and C–O–C bonds, respectively, whilst the MBi showed a slight shift in this value to appear at 1590 and 1010 cm^{-1}, respectively, due to the stearic acid adsorpted on Bi surface. According to Wang et al. [29], the hydroxyl groups of adsorbed water from the atmosphere or the carboxylic acid groups show distinctive band at 3270 cm^{-1}. Conversely, the MBi displayed more novel bands that correspond to the identification bands of stearic acid chains. The peaks at 1410 and 1730 cm^{-1} corresponded to the C–O groups bending and the typical stretching vibration of the C=O groups. Furthermore, the bending and rocking vibration that characterizes the aliphatic chains of stearic acid is responsible for the band that emerged at 712 cm^{-1} [30]. Stearic acid was shown to have successfully adsorbed onto the Bi surface based on the FTIR spectra.

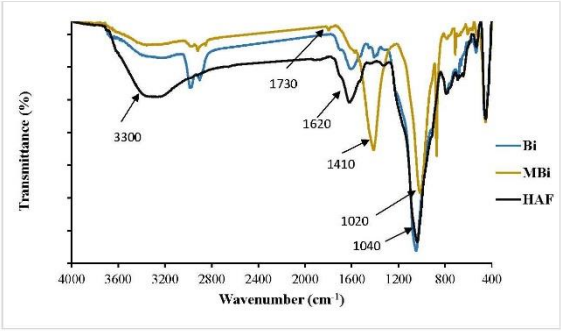

Figure 1: FTIR of Bi, MBi, and HAF

Fig. 2 displays the particle size distribution and water contact angle of different fillers. For Bi (Fig. 2A), two broad bands were shown with average particle sizes of 146 and 834 nm, and two broad bands for MBi (Fig. 2B) were obtained at 352 and 1179 nm. The formation of a thin layer of stearic acid on the surface of Bi was responsible for this increase in MBi's size which was proved by FTIR analysis, (**Fig. 1**). However, the HAF was only visible as a single narrow

peak, and its average particle size was 389 nm as illustrated in **Fig. 2C**.

Indeed, the water contact angle value of a material is related to its wettability. When this value is larger than 100°, the material is non-wettable, between 80° and 100° denote low wettability, between 60° and 80° are medium wettability, while less than 60° exhibits good wettability [31]. According to the findings, the water contact angle values of Bi, MBi, and HAF were 128.3°, 134.7°, and 138°, respectively (**Fig. 2**). The surface alteration of Bi produced by the stearic acid treatment may help to partially explain the observed disparity between the water contact angle for Bi and MBi.

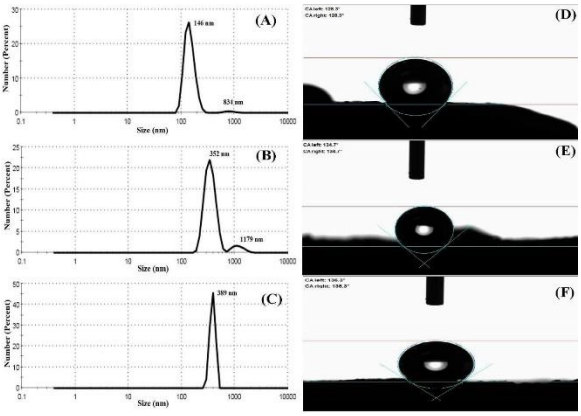

Figure 2: Particle size distribution (A, B, and C), and water contact angle (D, E, and F) of Bi, MBi, and HAF, respectively.

3.2 Characterizations of obtained EPDM composites

3.2.1 Rheometric characteristics

The biochar was added to the unvulcanized EPDM at different doses (10, 20, 30, and 40 phr). The standard procedure was followed to achieve the mixing process in a laboratory roll-mill. **Table 1** illustrates the rheological properties of the blended EPDM composites. From the findings, the rheometric characteristics exhibited a significant dependence on the biochar concentration, indicating that the vulcanization process is accelerated with higher biochar content. From the data presented in **Table 1**, it is evidenced that elastomeric compounds containing biochar exhibited the most minimal values for minimum torque (M_L) compared to those filled with HAF. This indicated that a more uniform final filler structure, in comparison to compounds incorporating HAF, might be obtained. Hence, this observation might suggest a reduced occurrence of rubber occlusion within the filler, as reflected by the lower viscosity values. In general, the ML values correlate with the compound's viscosity, which relies on the degree of processability of the compound's components [32, 33]. Notably, regardless of the elastomer utilized, filled MBi compounds demonstrated slightly lower ΔM values than those with HAF. However, this slight decrease did not impact the density of the crosslinks and the results contributed to the overall mechanical properties of the obtained HAF-filled EPDM compounds.

In addition, **Table 1** shows the elongation at break and tensile strength for the prepared EPDM composites. It is evident that the physicomechanical properties of the resulting vulcanizate rubber have improved with the addition of MBi to EPDM composites. In samples containing 10 phr MBi and 30 phr HAF (E6), the tensile strength values (10.7 Mpa) were somewhat higher compared to other composites. This can be explained as an increase in EPDM vulcanizates' rigidity. Conversely, as the concentration of biochar increased, the values of elongation at break increased marginally. This attests to the EPDM vulcanizates' increased rigidity. Furthermore, **Table 1** shows the swelling behaviour of EPDM vulcanizates versus the biochar content in toluene. The swelling readings have been shown to have somewhat risen. The chemical nature of MBi might be the cause of this. Conversely, there is a decrease in the soluble percentage in toluene. The way that the rubber and its components interact with the MBi could be the cause of this.

Table 1. The chemical recipe as well as the rheological and mechanical characteristics of prepared EPDM-composites.

Samples	**E1**	**E2**	**E3**	**E4**	**E5**	**E6**	**E7**	**E8**
	Chemical recipe (phr)							
EPDM	100	100	100	100	100	100	100	100
HAF	----	40	----	----	----	30	20	10
MBi	----	----	10	20	40	10	20	30
	Rheometer characteristic							
M_H (dNm)	14	24	15.68	16.2	19.6	23.3	22.7	20.8
M_L (dNm)	2.14	3.02	2.24	2.37	2.44	2.48	3.12	3.05
ΔM	11.88	21.01	13.44	13.81	17.15	20.8	19.62	17.75
t_{C90} (min)	40.3	24	33.9	38.5	31.2	32	28.1	29.9
t_{S2} (min)	19.5	6.37	13.8	17.9	9.32	5.86	9.05	10.5
CRI (min^{-1})	15.08	16.72	21.41	19.69	19.49	26.74	27.25	29.41
Tensile strength (Mpa)	6.22	10.1	7.88	8.12	8.77	10.7	9.55	9.17
Elongation at break (%)	495	570	554	564	600	576	612	644
Modulus (Mpa)	1.33	2.97	1.35	1.5	1.55	2.53	2.3	1.7
Equilibrium swelling (%)	218	152	222	198	178	149	153	169
Soluble fraction (%)	4.19	4.86	6	5.57	4.84	5.75	3.87	5.54

Basic recipe: (stearic acid 2 g, ZnO 5 g, Antioxidant 1.5 g, DOP 2 g, CBS 0.8 g, and sulfur 1.5 g).

3.2.1.1. Vulcanization kinetics study

To determine the obtained compounds curing characteristics, a rheometer was employed. While measuring the torque versus time, constant conditions were adjusted; temperature 152°C, frequency 1.6 Hz, and strain 0.5°. This data can provide valuable insights into various kinetic parameters such as the optimum cure time, cure rate index, degree of cross-linking or conversion, and activation energy [34].

Fig. 3A illustrates the vulcanization curves of EPDM at 152°C. These curves reveal three distinct regions of rubber cure in a typical accelerated sulfur vulcanization process . By analyzing the vulcanization curves and studying the torque as a function of time data, valuable insights can be gained regarding the curing process of the EPDM compound. This information allows for optimization of the cure time, understanding the rate of cross-linking, and determining the degree of conversion associated with the curing reaction [35]. The results revealed that increasing the MBi filler upload resulted in a fast cure rate or mitigated the optimum curing time (**Fig. 3A and Table 1**). As a result, the existence of MBi not only did not impede the vulcanization process but also accelerated it, without extending the tc90.

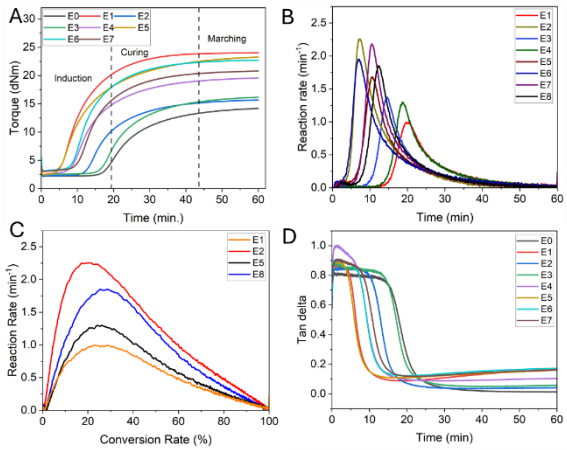

Figure 3: (**A**) Vulcanization curve, (**B**) reaction rate versus time, (**C**) reaction rate as a function of conversion for EPDM compounds E0, E1, E4, and E7, as well as (**D**) Loss tan delta as a function of curing time for vulcanized elastomeric compounds E0–E7.

By utilizing experimental data for analysis, the optimum curing time can be assessed. The degree of conversion (α) in the curing reaction was automatically calculated by MDR and it is defined as follows [36]:

$$\alpha = \frac{M_t - M_H}{M_H - M_L} \qquad \textbf{Eq. 4}$$

Where, M_H and M_L are the maximum and the minimum torque values, respectively, while *Mt* is the torque value at the given time of curing.

Fig. 3B plots dα/dt against time for EPDM at constant temperature 152 °C and different filler upload ratios (**Table 1**). Over time, the reaction rate increased until it reached the optimum and rapidly declined to the baseline forming an inverted bell-shaped curve [35]. Consequently, the cure rate increased with increasing the MBi loading ratio (**Fig. 1A**). Furthermore, **Fig. 3C** depicts the cure rate of EPDM compounds as a function of the conversion rate. The maximum value of the cure rate depicted between conversion is 0.2 and 0.4. Moreover, the dynamic time sweep (Tan delta) was also assessed (**Fig. 3D**). In terms of energy absorption and dispersion, tan delta (δ) measures how well a material absorbs and disperses energy [37, 38]. Consequently, changes in tangent δ can indicate alterations in the material's viscoelastic properties. From the findings, the presence of HAF and MBi remarkably elevated the value of tangent δ in the obtained EPDM composite. Therefore, this increase in tangent δ suggested an increase in the material's ability to dissipate energy that in turn potentially indicated an improved damping or flexibility.

3.2.2 Aging of rubber vulcanizates

The impact of biochar on the aging properties of EPDM vulcanizates was investigated. The EPDM vulcanizates were subjected to high thermal ageing for seven days at 90 ºC in a good air circulation oven. The aged samples' physicomechanical properties are represented in **Fig. 4,** which shows the measured values of elongation at break and tensile strength for each ageing period. The results illustrated a sustainable enhancement in the tensile strength, and a pronounced increase for the vulcanizates E0 and E7 was achieved, in which 50% to 71% was recorded, respectively (**Table 1** & **Fig. 4A**). Consequently, the findings indicated a progressive decline in both elongation and fracture stress of the rubber as aging time and temperature increased (**Fig. 4B**).

Significantly, the findings articulated that biochar-filled EPDM vulcanizates possessed high efficacy in shielding the elastomer from thermal aging and thus prolonged the shelf lifetime. Intriguingly, the resultant mechanical properties coincided with that obtained from the rheology measurements. Therein, rheology and mechanical findings gave compelling evidence about the impressive function associated with the as-prepared biochar-filled elastomer.

The soluble fraction (SF) of as-prepared composites is shown in **Fig. 4C**. Notably, the SF values did not significantly increase for any of the specimens under examination; E6 had the highest observed value, which reached 127% on the seventh day. Per Horikx's theory, the increase in the soluble fraction is more conspicuous and occurs more readily during the breakdown of the main chain [39, 40]. Consequently, larger segments are released using this procedure with fewer breakages than the SF obtained through eclectic crosslink rupture. Because of this, there were fewer breakages over time, keeping the chains' crosslinks intact.

Furthermore, a swelling test was conducted to evaluate the synergism between the filler and the elastomer matrix [41]. This analysis was done using

the swelling ratio, which is calculated by calculating the amount of solvent absorbed per unit weight of rubber. **Fig. 4D** shows how changing the MBi/HAF loading ratio affects the proportion of retained swelling in EPDM composites that are filled and unfilled. The results delineated a consistent pattern in the swelling ratio values over time post-MBi loading. Based on the data, it was inferred that toluene penetration into MBi-filled EPDM composites per sample stayed mostly consistent, independent of the amount of time that passed after MBi loading. On the other hand, the swelling ratio of pure EPDM showed a decreasing trend over time. Hence, it can be deduced that, despite the diverse amounts of MBi loading, there was no discernible impediment to toluene penetration into the filled EPDM composites throughout the experimental duration.

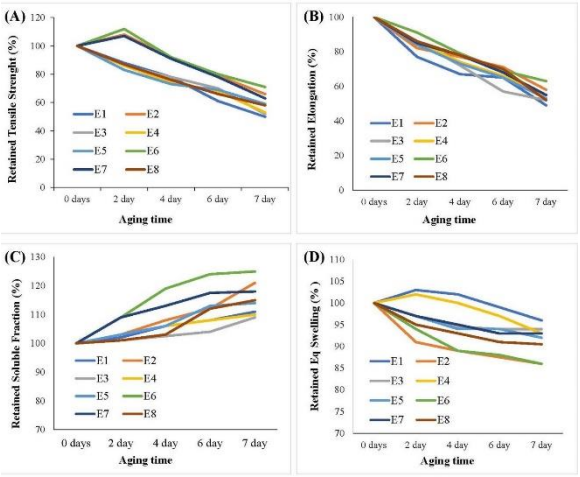

Figure 4: Thermal aging effect on: (**A**) retained tensile strength, (**B**) retained elongation, (**C**) retained soluble fraction, and (**D**) equilibrium swelling over time from 0-7 days.

3.2.3. FTIR analysis

The FTIR spectra of vulcanized EPDM composites were displayed in **Fig. 5** within the wavelength range of 400–4000 cm^{-1}. The symmetric and asymmetric stretching vibrations of C-H were responsible for the absorption peak observed in the pure EPDM rubber, which was measured at 2917 cm^{-1} and 2850 cm^{-1}, respectively. In addition, the C-H vibrations in -CH_2- and -CH_3 groups appear at 1461 and 1395 cm^{-1}, respectively [42]. Furthermore, the alkene (C=C) and carbonyl (C=O) were found to be stretching at 1730 and 1625 cm^{-1}, respectively [43]. EPDM composites spectrum demonstrated all the distinctive bands denoted in the pure EPDM counterpart. Notably, no new discriminative bands or band-shifting for the obtained composite spectra were noticed. Furthermore, the EPDM composites; E2, E5, and E7, exhibited the characteristic bands correspondence to both MBi and HAF. These discriminating FTIR spectra verified the physical dispersion of utilized fillers within the EPDM matrix. (**Fig. 5**).

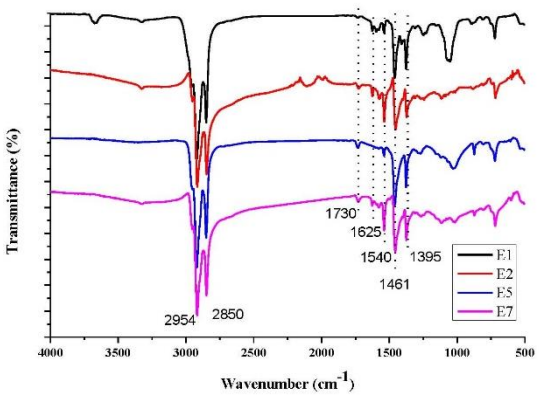

Figure 5: FTIR spectra for composites E1, E2, E5, and E7

3.2.4. Thermal analysis

The reactions and thermal characteristics of EPDM composites; E1, E2, E5, and E7, were assessed over varying temperatures throughout the study. (**Fig. 6**). The findings indicated that a single phase of heat degradation occurred in all composites. On the other hand, the E1 composite had the lowest ultimate weight at 500 °C and 22% solid residue left over. At 420 °C, the EPDM composites E2, E5, and E7 started to break down, and at 510 °C, the rate of weight loss was at its highest. According to the findings, composite E2 outperformed composite E5 in terms of thermal stability. Of the solid residue from E2 and E5, 34% and 41%, respectively, remained after heating to 580 °C. This proved that, in terms of the thermal degradation mechanism, HAF and MBi have comparatively identical effects on EPDM composites. Comparing the composite E7 to E2 and E5, on the other hand, it demonstrated a moderate level of thermal stability and had a 38% solid residual residue. In fact, there hasn't been any significant difference seen between the biochar-filled elastomer and its HAF equivalent.

Furthermore, DSC profiles of the obtained EPDM composite were also presented (**Fig. 6B)**. The profiles reveal an endothermic reaction correlated with TGA thereof all the prepared EPDM composites showed an endothermic horizontal step at 470 °C due to the decomposition of EPDM rubber.

3.2.5 Scanning Electron Microscopy Characterization

The dispersion of the applied fillers (MBi and HAF) in the elastomer matrix was investigated using SEM analysis, where the structural properties and the morphology of the EPDM composites (E1, E2, E5, and E7) were represented in **Fig. 7**. The composite E5 elaborated that although the MBi particles were randomly orientated; they were uniformly dispersed along the whole length of the observed matrix. The matrix morphology in the composite containing MBi showcased no signs of a phase-separated blend. Superior reinforcing for the EPDM composite was supplied by HAF, a smaller and more uniform

spherical particle, during the vulcanization process. Consequently, the HAF fillers appear to be dispersed more uniformly in the matrix than that of MBi because of the greater surface energy of HAF particles.

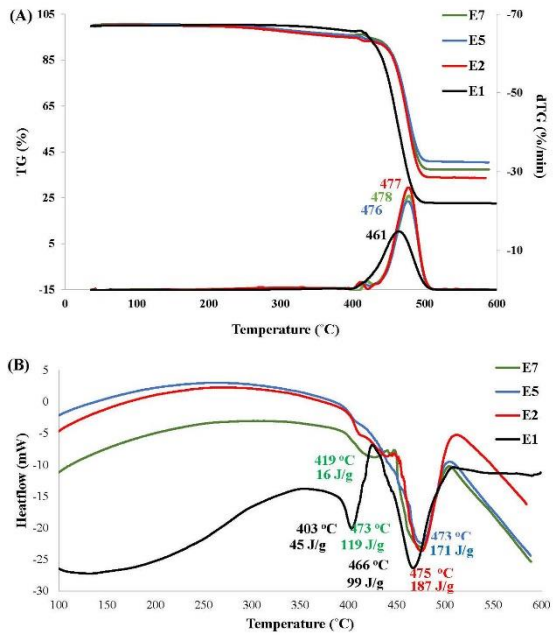

Figure 6: TG and DTG (A), and DSC (B) profiles of E1, E2, E5, and E7

3.2.6 Water and oxygen permeability

Table 2 illustrates WVTR and OTR values for the obtained composites; E1, E2, E5, and E7. Pure EPDM exhibited elevated OTR and WVTR with values of 713 cc/m^2. d and 5.8 g/m^2.d, respectively. The introduction of fillers whether HAF (E2), MBi (E5), or a combination of both (E7), resulted in a decrease in these values. This implies that HAF/MBi fillers occupy some of the pores within the elastomer. Notably, composite E2 exhibited the lowest OTR and WVTR compared to E5, suggesting that the smaller size of HAF (146 nm) in addition to its greater hydrophobicity compared to MBi (389 nm) played a key role in the improvement of the results (**Fig. 8).**

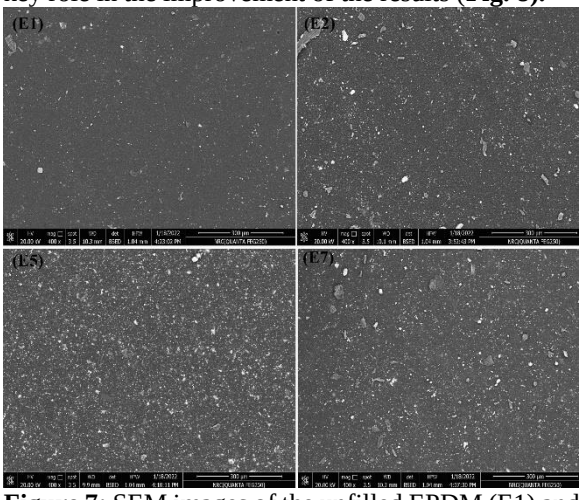

Figure 7: SEM images of the unfilled EPDM (E1) and composites E2, E5, and E7.

Table 2: Water and oxygen permeability for E1, E2, E5, and E7

Composites	OTR (cc/m^2.d)	WVTR (g/m^2.d)
E1	713	5.8
E2	427	4.5
E5	614	4.7
E7	515	4.3

3.2.7 Acoustic behaviour

Fig. 8 depicts the sound absorption levels within the frequency range of 500 to 6000 Hz for the obtained composites: E1, E2, E5, and E7. The absorption coefficient (α) of the rubber composite is notably influenced by the presence and the type of filler employed. Enhanced sound absorption in rubber is evident within the frequency range of 3000–4000 Hz, where α experienced a substantial increase, peaking at 4000 Hz with α = 0.32. Beyond 4000 Hz, sample E1 demonstrates a decrease in α, indicating its ability to absorb noise at a level lower than 0.32. In contrast, the filled EPDM (E2, E5, and E7) exhibited α with values less than 0.1, although there is an increase in this value at a frequency within the range of 5000–6000 Hz to reach an optimum value of 0.42.

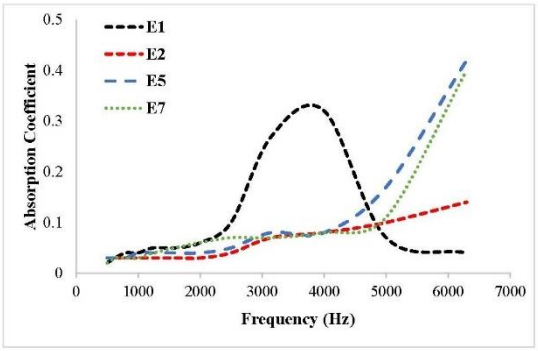

Figure 8: Sound absorption coefficient for E1, E2, E5, and E7

3.3 Dielectric spectroscopy investigations

3.3.1 Dielectric constant

The permittivity, ε′, is determined for pure vulcanized EPDM rubber and the obtained composites (**Fig. 9)**. From the findings, it was verified that the electrical insulation features of the vulcanized EPDM were not affected remarkably by the incorporation of biochar particles to EPDM at 10 and 20 phr as ε′ for the obtained composites. In turn, E1, E3, and E4 collapsed together and possessed nearly the same value (ε′ ~ 3.5). For composite E5, a slight increase in the permittivity over all the considered frequency windows has been displayed. Although there was a slight decrease of permittivity with increasing frequency in the E5 sample, the permittivity could be considered stable all over the investigated frequency. Since there is a small dispersion step that could be notified at the highest frequency window, it was

anticipated that a very small dynamic relaxation peak in the dielectric loss spectrum would accompany this step. On the other hand, it was observed that the addition of HAF massively improved the permittivity of the composite.

The data analysis revealed that composite E2 exhibited elevated permittivity compared to all other composites. To facilitate comparison, we focus on the permittivity values at a specific frequency point, namely 1 kHz. Specifically, E2 demonstrated a permittivity value of 8.79. On the other hand, E6 led to a reduction in permittivity to 6.93. Furthermore, this value decreased even further to 6.15 for composite E7. All the results obtained intensively correlated with the results obtained from the rheology and thermal measurements.

3.3.2 AC-Conductivity

The dielectric spectra of both the pure rubber and the obtained composites can be effectively characterized by the complex conductivity, σ*. This parameter is utilized to assess, alongside the complex conductivity function (σ*(ν)) and the complex dielectric function (ε*(ν)). While these two parameters are equivalent, they highlight distinct aspects of the material's electrical properties [44-46].

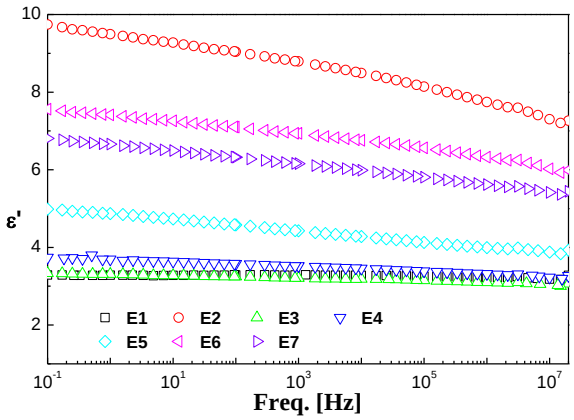

Figure 9: The dielectric constant, ε′, of the prepared composites E1-E7.

In **Fig. 10,** the graphical representation illustrates the real part of the complex conductivity, σ'; also referred to as ac-conductivity or σac, as a function of frequency spanning from 0.1 Hz to 20 MHz at the ambient temperature for EPDM composites; E1, E2, E5, and E7. The observed linear decline on a log-log scale with decreasing frequency indicates that all four composites exhibited characteristics consistent with perfect insulation behaviour [38, 47]. Nevertheless, there is a marginal rise in ac-conductivity, approximately one decade at 0.1 Hz, which is attributed to the presence of the uploaded HAF/MBi. Despite this effect, all four examined samples are deemed perfect insulators, and the substitution of MBi for HAF does not yield any significant impact. As a result, this finding addresses the primary objective of this study, whereby it indicated the feasibility of replacing carbon black with MBi as an environmentally friendly and sustainable filler, particularly in applications related to electrical technology.

The dielectric dissipation factor, commonly referred to as the loss tangent [$\tan\delta = \varepsilon''/\varepsilon'$]), is graphically depicted against frequency in the inset of **Fig. 10**. In the same vein, the dissipation factor exhibits stability against frequency, persisting until around 1 kHz and beyond, even with the addition of the HAF/MBi. The abrupt increase of about one decade of the plateau value from 0.001 to 0.01 was exhibited after examining the filled EPDM. However, this slight elevation had no great impact and the yield values remained within a reasonable range for typical electrical insulators. At relatively higher frequencies, a peak-like behaviour accompanied by a small dispersion step was observed and it is assumed that this phenomenon was due to some specific polarization. The origin and characteristics of this dynamic process are currently beyond the scope of the present study; however, further investigations are warranted to explore and understand this relaxation process.

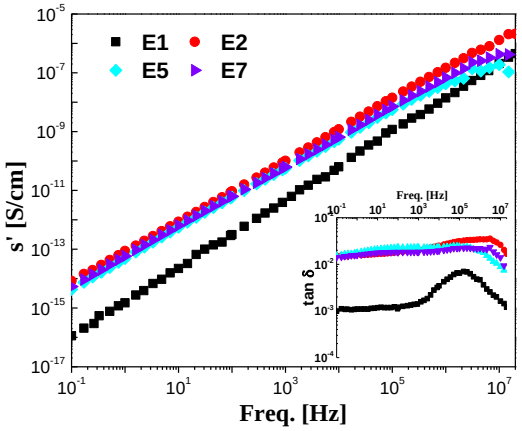

Figure 10: The frequency dependence of the ac-conductivity, σ′, as presented against frequency for E1, E2, E5, and E7. The inset shows a similar illustration for the loss tangent, tan δ.

4. Conclusion

In this study, biochar derived from citrus tree agricultural waste was modified with stearic acid to enhance its surface hydrophobicity. The modified biochar (MBi) demonstrated an improved synergy with elastomer and did not impede the vulcanization process; instead, it accelerated it, leading to reduced energy consumption and processing costs. Moreover, rheological tests confirmed the positive effects on vulcanization without extending the tc90. For thermogravimetric analysis, a higher thermal stability in the biochar-filled composites compared to pure EPDM has been obtained. The composites also exhibited lower oxygen and water permeability, as well as improved resistance to thermal aging and

swelling. In the same stream, electric conductivity assessments and SEM analysis indicated that the uniform dispersion of modified biochar particles contributed to increased permittivity, transforming the composites into effective electrical insulators. Overall, the study suggests that MBi can be considered safe filler with no detrimental effects on EPDM, offering potential as a replacement for traditional fillers like HAF in industrial applications.

References

1. Pourmand P., Hedenqvist M.S., Furó I., and Gedde U.W., Deterioration of highly filled EPDM rubber by thermal ageing in air: Kinetics and non-destructive monitoring. *Polymer Testing*, **64**, 267-276 (2017).
2. Planes E., Chazeau L., Vigier G., Fournier J., and Stevenson-Royaud I., Influence of fillers on mechanical properties of ATH filled EPDM during ageing by gamma irradiation. *Polymer Degradation and Stability*, **95**, 1029-1038 (2010).
3. Tomer N.S., Delor-Jestin F., Singh R.P., and Lacoste J., Cross-linking assessment after accelerated ageing of ethylene propylene diene monomer rubber. *Polymer Degradation and Stability*, **92**, 457-463 (2007).
4. Fan Y., Fowler G.D., and Zhao M., The past, present and future of carbon black as a rubber reinforcing filler – A review. *Journal of Cleaner Production*, **247**, 119115 (2020).
5. Abd El-Aziz M.E., Shafik E.S., Tawfic M.L., and Morsi S.M.M., Biochar from waste agriculture as reinforcement filer for styrene/butadiene rubber. *Polymer Composites*, **43**, 1295-1304 (2021).
6. Gatos K.G., Thomann R., and Karger-Kocsis J., Characteristics of ethylene propylene diene monomer rubber/organoclay nanocomposites resulting from different processing conditions and formulations. *Polymer International*, **53**, 1191-1197 (2004).
7. Mensah B., Kang S.I., Wang W., and Nah C., Effect of graphene on polar and nonpolar rubber matrices. *Mechanics of Advanced Materials and Modern Processes*, **4**, 1-12 (2018).
8. Choi E.Y., Kim C.K., and Park C.B., Fabrication of MA-EPDM grafted MWCNTs by reactive extrusion for enhanced interfacial adhesion and mechanical properties of PP/MA-EPDM composite. *Composites Part B: Engineering*, **242**, 110043 (2022).
9. Ning N., Ma Q., Zhang Y., Zhang L., Wu H., and Tian M., Enhanced thermo-oxidative aging resistance of EPDM at high temperature by using synergistic antioxidants. *Polymer Degradation and Stability*, **102**, 1-8 (2014).
10. Do J.H., Kim D.Y., and Seo K.H., Effect of eco-friendly inorganic flame retardants on mechanical and flame-retardant properties of EPDM compound. *Elastomers and composites*, **55**, 40-45 (2020).
11. Arroyo M., López-Manchado M.A., Valentín J.L., and Carretero J., Morphology/behaviour relationship of nanocomposites based on natural rubber/epoxidized natural rubber blends. *Composites Science and Technology*, **67**, 1330-1339 (2007).
12. Zeid M.M.A., Radiation effect on properties of carbon black filled NBR/EPDM rubber blends. *European Polymer Journal*, **43**, 4415-4422 (2007).
13. Rattanasupa B., and Keawwattana W., The development of rubber compound based on natural rubber (NR) and ethylene-propylene-diene-monomer (EPDM) rubber for playground rubber mat. *Agriculture and Natural Resources*, **41**, 239-247 (2007).
14. Zhang Y., He M., Wang L., Yan J., Ma B., Zhu X., Ok Y.S., Mechtcherine V., and Tsang D.C.W., Biochar as construction materials for achieving carbon neutrality. *Biochar*, **4**, 59 (2022).
15. Sakhiya A.K., Anand A., and Kaushal P., Production, activation, and applications of biochar in recent times. *Biochar*, **2**, 253-285 (2020).
16. Lu L., Yu W., Wang Y., Zhang K., Zhu X., Zhang Y., Wu Y., Ullah H., Xiao X., and Chen B., Application of biochar-based materials in environmental remediation: from multi-level structures to specific devices. *Biochar*, **2**, 1-31 (2020).
17. Dehkhoda A.M., Gyenge E., and Ellis N., A novel method to tailor the porous structure of KOH-activated biochar and its application in capacitive deionization and energy storage. *Biomass and Bioenergy*, **87**, 107-121 (2016).
18. Qiu M., Liu L., Ling Q., Cai Y., Yu S., Wang S., Fu D., Hu B., and Wang X., Biochar for the removal of contaminants from soil and water: a review. *Biochar*, **4**, 19 (2022).
19. Gao Y., Fang Z., Van Zwieten L., Bolan N., Dong D., Quin B.F., Meng J., Li F., Wu F., Wang H., and Chen W., A critical review of biochar-based nitrogen fertilizers and their effects on crop production and the environment. *Biochar*, **4**, 36 (2022).
20. Yang R., Guo X., Wu H., Kang W., Song K., Li Y., Huang X., and Wang G., Anisotropic hemp-stem-derived biochar supported phase change materials with efficient solar-thermal energy conversion and storage. *Biochar*, **4**, 38 (2022).
21. Abd Elwahed M.S., Abd El-Aziz M.E., Shaaban E.A., and Salama D.M., New trend to use biochar as foliar application for wheat plants (*Triticum Aestivum*). *Journal of Plant Nutrition*, **42**, 1180-1191 (2019).
22. Salama D.M., Abd El-Aziz M.E., El-Naggar M.E., Shaaban E.A., and Abd El-Wahed M.S., Synthesis of an eco-friendly nanocomposite fertilizer for common bean based on carbon nanoparticles from agricultural waste biochar. *Pedosphere*, **31**, 923-933 (2021).

23. Abd El-Aziz M., Youssef A., Kamel S., and Turky G., Conducting hydrogel based on chitosan, polypyrrole and magnetite nanoparticles: a broadband dielectric spectroscopy study. *Polymer Bulletin*, 1-20 (2018).
24. Youssef A.M., Hasanin M.S., Abd El-Aziz M.E., and Turky G.M., Conducting chitosan/hydroxylethyl cellulose/polyaniline bionanocomposites hydrogel based on graphene oxide doped with Ag-NPs. *International Journal of Biological Macromolecules*, **167**, 1435-1444 (2021).
25. El-Sayed N.S., Moussa M.A., Kamel S., and Turky G., Development of electrical conducting nanocomposite based on carboxymethyl cellulose hydrogel/silver nanoparticles@ polypyrrole. *Synthetic Metals*, **250**, 104-114 (2019).
26. Morsi S.M.M., El-Aziz M.E.A., Morsi R.M.M., and Hussain A.I., Polypyrrole-coated latex particles as core/shell composites for antistatic coatings and energy storage applications. *Journal of Coatings Technology and Research*, **16**, 745-759 (2019).
27. Ahmed K., Nizami S.S., Raza N.Z., and Shirin K., Cure Characteristics, Mechanical and Swelling Properties of Marble Sludge Filled EPDM Modified Chloroprene Rubber Blends. *J Advances in Materials Physics and Chemistry*, **2**, 90-97 (2012).
28. Ahmed K., Nizami S.S., Raza N.Z., and Mahmood K., Mechanical, swelling, and thermal aging properties of marble sludge-natural rubber composites. *International Journal of Industrial Chemistry*, **3**, 21 (2012).
29. Wang L., Wang Y., Li A., Yang Y., Tang Q., Cao H., Qi T., and Li C., Electrocatalysis of carbon black- or poly(diallyldimethylammonium chloride)-functionalized activated carbon nanotubes-supported Pd–Tb towards methanol oxidation in alkaline media. *Journal of Power Sources*, **257**, 138-146 (2014).
30. Chen Y., Zhang X., Wang B., Lv M., Zhu Y., and Gao J., Fabrication and characterization of novel shape-stabilized stearic acid composite phase change materials with tannic-acid-templated mesoporous silica nanoparticles for thermal energy storage. *RSC Advances*, **7**, 15625-15631 (2017).
31. Benkreif R., Brahmia F.Z., and Csiha C., Influence of moisture content on the contact angle and surface tension measured on birch wood surfaces. *European Journal of Wood and Wood Products*, **79**, 907-913 (2021).
32. Ribeiro W.B., Bérti G.B., Faccio M., Godinho M., and Brandalise R.N., Evaluation of Biochar Production Temperature in Interaction with Elastomers of Different Polarities. *Materials Research*, **26**, e20220341 (2023).
33. Hiranobe C.T., Ribeiro G.D., Torres G.B., Reis E.A.P.d., Cabrera F.C., Job A.E., Paim L.L., and Santos R.J.d., Cross-linked density determination of natural rubber compounds by different analytical techniques. *Materials Research*, **24**, e20210041 (2021).
34. Rosca I.D., and Vergnaud J.M., Study of process of cure of EPDM rubbers in moving die rheometer. *Plastics, Rubber and Composites*, **30**, 275-281 (2001).
35. Fathurrohman M.I., Maspanger D.R., and Sutrisno S., Vulcanization kinetics and mechanical properties of ethylene propylene diene monomer thermal insulation. *Bulletin of Chemical Reaction Engineering & Catalysis*, **10**, 104 (2015).
36. Leroy E., Souid A., and Deterre R., A continuous kinetic model of rubber vulcanization predicting induction and reversion. *Polymer Testing*, **32**, 575-582 (2013).
37. Khimi S.R., and Pickering K.L., A new method to predict optimum cure time of rubber compound using dynamic mechanical analysis. *Journal of Applied Polymer Science*, **131** (2014).
38. Koriem A.A., Abd El-Aziz M.E., Salem S.R., Hussain A.I., and Turky G., Management of agricultural waste to manufacture biochar: An alternative reinforcing filler for carbon black in nitrile butadiene rubber composites. *Journal of Cleaner Production*, **428**, 139360 (2023).
39. Dorigato A., Rigotti D., and Fredi G., Recent advances in the devulcanization technologies of industrially relevant sulfur-vulcanized elastomers. *Advanced Industrial and Engineering Polymer Research*, **6**, 288-309 (2023).
40. Horikx M.M., Chain scissions in a polymer network. *Journal of Polymer Science*, **19**, 445-454 (1956).
41. Ghosh P., and Chakrabarti A., Conducting carbon black filled EPDM vulcanizates: assessment of dependence of physical and mechanical properties and conducting character on variation of filler loading. *European Polymer Journal*, **36**, 1043-1054 (2000).
42. Riba Ruiz J.R., Canals T., and Cantero R., Supervision of Ethylene Propylene Diene M-Class (EPDM) Rubber Vulcanization and Recovery Processes Using Attenuated Total Reflection Fourier Transform Infrared (ATR FT-IR) Spectroscopy and Multivariate Analysis. *Applied spectroscopy*, **71**, 141-151 (2017).
43. Kondyurin A. EPDM Rubber Modified by Nitrogen Plasma Immersion Ion Implantation, In *Materials*, (2018).
44. Youssef A., Abd El-Aziz M., El-Sayed E., Abdel-Aziz M., El-Hakim A.A., Kamel S., and Turky G., Morphological, Electrical & Antibacterial properties of Trilayered Cs/PAA/PPy bionanocomposites hydrogel based on Fe_3O_4-NPs. *Carbohydrate polymers*, **196**, 483-493 (2018).
45. Margha F.H., El-Bassyouni G.T., and Turky G.M., Enhancing the electrical conductivity of vanadate

glass system (Fe2O3, B2O3, V2O5) via doping with sodium or strontium cations. *Ceramics International*, **45**, 11838-11843 (2019).
46. Abdel-Baki M., Mostafa A.M., Fayad A.M., El-Bassyouni G.T., and Turky G.M., Improving the optical, electrical, and dielectric characteristics of MgO doped borate glass for optoelectronic applications. *Journal of Applied Physics*, **133**, 065102 (2023).
47. El-Adly R.A., and Turky G.M., Comparative study between prepared electrical grease and the imported one. *Egyptian Journal of Petroleum*, **27**, 209-213 (2018).